Trop J Nat Prod Res, July 2023; 7(7):3421-3432 **ISSN 2616-0684 (Print)**
ISSN 2616-0692 (Electronic)

Tropical Journal of Natural Product Research

Available online at https://www.tjnpr.org

Original Research Article

Combinatory *in silico* Study on Anti-Diabetic Potential of *Ganoderma lucidum* Compounds Against *α*-Glucosidase

Nguyen P.D. Nguyen[1], Phan T. Quy[1], Dao C. To[2], Thanh Q. Bui[3], Nguyen V. Phu[4], Tran T. A. My[3], Phi H. Nguyen[5], Nguyen H. Kien[1], Nguyen T. T. Hai[3], Nguyen T. A. Nhung[3]*

[1]*Tay Nguyen University, Buon Ma Thuot, Dak Lak 630000, Vietnam*
[2]*Phenikaa University Nano Institute (PHENA), Phenikaa University, Yen Nghia, Ha Dong district, Hanoi 12116, Vietnam*
[3]*Department of Chemistry, University of Sciences, Hue University, Hue City 530000, Vietnam*
[4]*Faculty of Basic Sciences, University of Medicine and Pharmacy, Hue University, Hue 530000, Vietnam*
[5]*Institute of Natural Products Chemistry, Vietnam Academy of Science and Technology (VAST), 18 Hoang Quoc Viet, Cau Giay district, Hanoi 122100, Vietnam*

ARTICLE INFO

Article history:
Received 01 June 2023
Revised 21 June 2023
Accepted 10 July 2023
Published online 01 August 2023

ABSTRACT

Ganoderma species is excessively well-known for a variety of medicinal effects and health benefits by folk experiences, thus often underestimated for componential specification. *Ganoderma lucidum* methanol-extracted components (1-15) were selected from the literature and subjected for computational evaluations on the anti-diabetic potentiality. As the results, molecular docking simulation suggests the most promising PDB-3W37 (α-glucosidase) inhibitors from the standpoint of static intermolecular interaction, i.e. 1 (DS -12.8 kcal.mol^{-1}; RMSD 1.23 Å) > 2 (DS -12.3 kcal.mol^{-1}; RMSD 1.76 Å) > 11 (DS -12.0 kcal.mol^{-1}; RMSD 1.20 Å) ≈ 13 (DS -12.1 kcal.mol^{-1}; RMSD 1.58 Å); QSARIS confirm their biocompatibility given the physicochemical properties in reference to Lipinski's rule of five; ADMET pharmacokinetics and pharmacology justify their pharmaceutical applicability. Quantum-based retrievals justify their suitability from the view of intrinsic chemical properties, i.e: ground-state energy, dipole moment, and band gap: 1 (-1888.85 eV; 9.129 Debye; 5.952 eV), 2 (-1887.64 eV; 6.689 Debye; 6.393 eV), 11 (-1961.62 eV; 5.106 Debye; 3.599 eV), 13 (-1543.14 eV; 8.294 Debye; 4.598 eV). The results encourage experimental attempts for anti-diabetic applications on 1 (Butyl lucidenate P), 2 (Butyl lucidenate E_2), 11 (Methyl ganoderate H), and 13 (Methyl lucidenate N).

Keywords: *Ganoderma lucidum*, α-glucosidase, density functional theory, molecular docking simulation, ADMET.

Introduction

Ganoderma species have been used in traditional medicine for over 2000 years.[1] The earliest document describes the beneficial effects of several mushrooms with a reference to the medicinal mushroom *Ganoderma lucidum* (Polyporaceae).[1] The fruiting part of *G. lucidum* is generally utilized in China, Korea, Vietnam, and Japan as an important and valuable traditional folk medicine, particularly in the treatment of asthma, chronic hepatitis, bronchitis, nephritis, joint pain, sleep deprivation, and stomach ulcers.[2] Many components have been found to have several important biological functions, e.g. antibacterial, HIV-resistant, tumor-inhibiting, cancer-preventive, anti-inflammatory, and diabetes-relieved potentials.[3–5] More than 400 bioactive compounds, primarily polysaccharides, triterpenes, and over 150 ganoderic acids, have been identified from mycelium, spores, and fruiting bodies of *G. lucidum*.[6,7] However, the large bioavailability and bio-versatility induce an almost prohibitive challenge to allocate the component-activity relationship from the view of experimental trials.

*Corresponding author. E mail: ntanhung@hueuni.edu.vn
Tel: +84986980263

Citation: Nguyen NPD, Quy PT, To DC, Bui TQ, Phu NV, My NTA, Nguyen PH, Kien NH, Hai NTT, Nhung NTA. Combinatory *in silico* Study on Anti-Diabetic Potential of *Ganoderma lucidum* Compounds Against α-Glucosidase. Trop J Nat Prod Res. 2023; 7(7):3421-3432 http://www.doi.org/10.26538/tjnpr/v7i7.21

Official Journal of Natural Product Research Group, Faculty of Pharmacy, University of Benin, Benin City, Nigeria.

Fortunately, prescreening research based on *in silico* techniques can provide effective solutions for medical science in general, and for *G. lucidum* in particular. For instance, the molecular docking simulation technique has been used extensively in drug-design science thanks to the its effectiveness in prediction of inhibitory conformation formed by small candidate ligands and targeted protein sites.[8] Given the most commonly accepted algorithms, the method estimates ligand-target binding pseudo-Gibbs free energy and intermolecular configurations, thus providing inhibitory effectiveness from the static stability of the duo systems. In principle, if effectively inhibited, it is likely that the targeted enzyme might bear conformational changes of significance, thus resulting in loss of enzymatic functionality. In terms of α-glucosidase, the amount of glucose catalytically synthesised and released to the bloodstream is in turn reduced. This technique can be utilised together with statistically regressive models for physicochemical properties of the candidates, which can represent the pre-docking physio-chemical compatibility, to result in more experiment-correlated output. By the similar approach, ADMET (absorption, distribution, metabolism, excretion, and toxicity) parameters and pharmacokinetic properties of a chemical structure can be predicted, e.g. using SwissADME. Independently, *ab initio* implementations can provide the information on the chemical behaviour based on the electronic properties; consequently, theoretical arguments on intermolecular tendencies can be carried out. Altogether, a highly well-rounded prediction on the biological compatibility and pharmacological suitability of extensive counts of candidates can be assessed in a time-efficient manner.[9] To our knowledge, although there have been researches focusing on the anti-α-glucosidase effects of *G. lucidum*,[10–12] up to date there is no research using the molecular docking technique specifically to pay attention to the mechanism of isolated compounds from the mushroom. In this study, the candidates were

 ISSN 2616-0684 (Print)
ISSN 2616-0692 (Electronic)

selected from the methanol-based extracts found by different preceding reports as our preliminary screening for the solvent potential against diabetes in general. The information retrievable can serve as the justification for further experimental attempts. Table 1 summarises the bioactive compound subjected, which were found as the major bioactive compounds of the mushroom family or proven with practicable accumulative isolation.

Estimated ca. 1.5 million deaths in 2019 and predicted to be the sixth leading lethal cause by 2030,[21] the concern about diabetes mellitus (DM) is increasing worldwide. Type 1 and type 2 diabetes are most commonly diagnosed; in which, the former is tissue resistance to the pancreas-produced insulin while the latter refers to the low synthesis of insulin, both leading to the uncontrollability of blood-sugar levels.[10] Particularly, type 2 diabetes accounts for 90–95% of all cases; popularly, the primary pharmacological treatment for this type is bases on the retardation of glucose absorption, such as digestive α-glucosidase inhibition.[11] The exoenzyme is responsible for the catalysis of starch and disaccharides hydrolysis into monosaccharides, e.g. glucose.[22] Effective inhibitors against this protein would help slow the blood-sugar elevation after a carbohydrate-rich meal; hence, α-glucosidase has been considered one of the most potential targets for diabetic treatments.[23] The biological assembly of *α*-glucosidase extracted from *Beta vulgaris* was well-characterised and deposited to the protein data bank (RCSB PDB) under the entry PDB-3W37 (DOI: 10.2210/pdb3W37/pdb).

Acarbose was the first approved substance (AGI) as an α-glucosidase inhibitor and commonly prescribed for postprandial intake. Its effectiveness to reduce the absorption of glucose from carbohydrate-containing foods was well-proven by clinical research. The medicine has been shown to provide euglycemia, in part by increasing GLP-1 levels and reducing postprandial spikes in glucose and lipid levels.[24] However, the controlled drug was recently reported to be connected to the maintenance of stable blood glucose levels afterwards.[25] Furthermore, although administered via the oral route, acarbose acts in the gastrointestinal tract with very low systematic bioavailability; quantitatively, there is ca. 2 % absorbed of the taken drug by the intestine as the active drug.[26] Therefore, it is still in need to search for alternative glucose-lowering agents with elevated pharmacological efficacy and biological compatibility. Natural sources are considered highly promising.

In this work, a combination of computer-based platforms was designed as an in-depth theoretical argument on anti-diabetic potential of *G. lucidum*-extracted components as α-glucosidase inhibitors. The chemical knowledge is collected from preceding studies to serve as computaional input in this work.

Table 1: Selected bioactive compounds in *G. lucidum* extracts

Notation	Subtance	Reference
1	Butyl lucidenate P	4
2	Butyl lucidenate E2	4
3	Butyl lucidenate D2	4
4	Butyl lucidenate Q	4
5	Ergosterol	13
6	Stellasterol	14
7	Ergosterol peroxide	15
8	Ganoderiol F	16
9	Lucidumol B	17
10	Ganodermanondiol	17
11	Methyl ganoderate H	13
12	Methyl ganoderate J	18
13	Methyl lucidenate	19
14	Methyl lucidenate A	20
15	Butyl lucidenate N	19

The candidates are subjected for evaluation of inhibitability (by molecular docking simulation), biocompatibility (by physicochemical properties), pharmaceutical potentiality (by pharmacokinetics and pharmacology), and intrinsic chemical tendency (by quantum calculation).

Methodology

Figure 1 shows the biological assembly of α-glucosidase (PDB-3W37; DOI: 10.2210/pdb3W37/pdb) and the structural formula of Acarbose (D); Figure 2 provides chemical formulae of ligands (1-15). These served as the input for a variety of computational plaforms, whose output are utilized for different theoretical arguments. In particular, docking-score values given by docking technique can represent the static inhibitory effectiveness of each ligand-protein complexes; QSARIS-based physicochemical properties of a candidate can be argued for its drug likeness in reference to Lipinski's thresholds; ADMET-based pharmacological properties of a compound can be justified for its medicinal potentiality based on Pires' interpretations; ground-state energy, dipole moment, and other electronic charateristics obtained from quantum calculation can provide the bio-chemical stability and bio-medium compatibility of a small-size structure.

Molecular docking simulation

A typical procedure of molecular docking simulation using Molecular Operating Environment (Version: MOE 2015.10 [27]) follows four steps [28–30] providing predictions on ligand-protein complex structures. First, input preparation was for the treatments of individual participants. Crystal structure of α-glucosidase (PDB-3W37; DOI: 10.2210/pdb3W37/pdb) was acquired from Protein Data Bank; active amino acids: within 4.5 Å to ligands; Tether-Receptor strength: 5000; energy resolution: 0.0001 kcal.mol^{-1}.Å^{-1}. Chemical formulae of ligands were from the experimental determination in this work; energy optimization: Conj Grad algorithm; energy-change termination: 0.0001 kcal.mol^{-1}; maximum interactions: 1000; empirical charge-assigning: Gasteiger-Huckel method. Second, ligand-protein inhibitory interactions were simulated, under docking configuration: retaining poses: 10; solutions per iteration: 1000; solutions per fragmentation: 200. Third, the formed complex structures were separated and re-docked, under re-docking iteration. The accuracy of the docking protocol is justified if RMSD values (of docked and re-docked conformations) are all under 2 Å. Finally, the interpretation of the obtained data can be given from theoretical views for the effectiveness of ligand-protein interactions. The primary indicators are docking score (DS) energy, equivalent to pseudo-Gibbs free energy (contributed by hydrophilic binding and hydrophobic interaction), and root-mean-square deviation (RMSD) value, representing geometrical complementarity (argued from the average distances between backbone atoms).

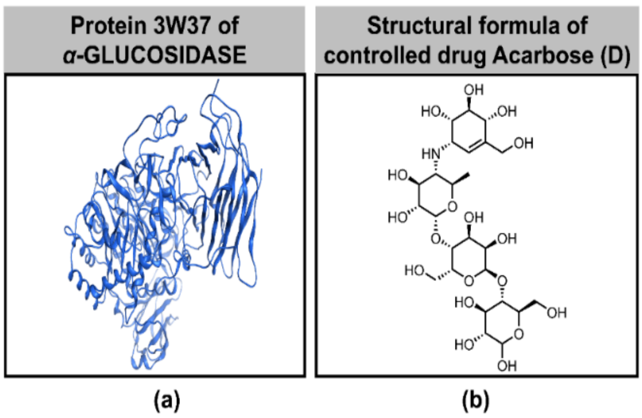

Figure 1: Crystal structure of (a) protein 3W37 of α-glucosidase; and (b) structural formula of commercial medicine for diabetes treatment Acarbose (D)

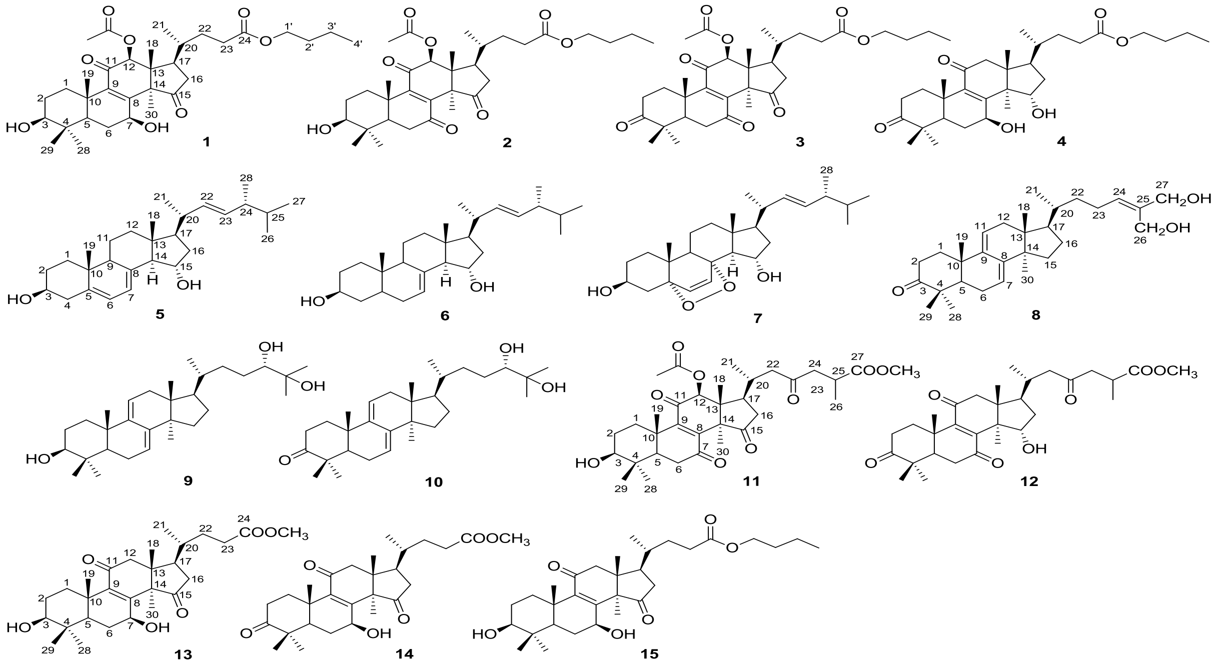

Figure 2: Chemical structure of selected compounds 1–15 from *G. lucidum* composition

QSARIS-based analysis

The physicochemical properties of the candidates were subjected for drug-like evaluation with the reference to Lipinski's rule of five[32]. Parameters: QSARIS-derived physical properties based on Gasteiger–Marsili method[31], including: molecular mass (Da), polarizability (Å^3) and size (Å), and dispersion coefficients (log*P* and log*S*). Criteria: (i) Molecular mass < 500 Da; (ii) hydrogen-bond donors ≤ 5; (iii) hydrogen-bond acceptors ≤ 10; (iv) log*P* < +5.

ADMET analysis

ADMET properties of the candidates were subjected for pharma-suitable evaluation with reference to the interpretations proposed by Pires *et al*..[33] The pharmacological and pharmacokinetic descriptors were given by SwissADME (http://www.swissadme.ch/; 1st May 2023).

Density functional theory calculation

Molecular optimised geometries and their quantum properties were calculated using Gaussian 09 (Version: IA32W-G09RevA.02) without symmetry constraints [34] based on density functional theory (DFT). Level of theory M052X and basis set def2-TZVPP were selected.[35] Vibrational frequencies were calculated to check the structural global minimum on the potential energy surface (PES). The frozen-core approximation for non-valence-shell electrons was applied for geometrical optimization; each run was under the resolution-of-identity (RI) approximation. The frontier orbital analysis was carried out by NBO 5.1 [36] at the level of theory M052X/def2-TZVPP. In theory, the highest occupied molecular orbital (HOMO) energy, i.e. E_{HOMO}, can be interpreted as the electron-denoting capability; in contrast, the lowest unoccupied molecular orbital (LUMO), i.e. E_{LUMO}, represents the accepting counterpart; energy gap $\Delta E = E_{\text{LUMO}} - E_{\text{HOMO}}$ typifies electric conductivity of the host molecule.

Hardware specifications

All the computational implementations were run on a personal workstation HP Z620: CPU Intel® Xeon® E5-2670 v2 3.30 GHz; RAM 48 GB 1600 MHz.

Results and Discussion

Ligand-3W37 inhibitability

Four sites most active to the selected ligands are presented in Figure 3, i.e. site 1 (grey), site 2 (blue), site 3 (orange), and site 4 (yellow); the primary data are summarised in Table 2, i.e. docking score (DS) values and the number of hydrogen bonds. Overall, the inhibitory agents with the highest inhibitory effects towards PDB-3W37 can be interpreted with the highest overall DS values, i.e. 1, 2, 11, 13 ($DS_{\text{overall}} < -10$ kcal.mol^{-1}). This preliminary consideration is of the fact that in theory, a good inhibitor can probably inhibit many different protein structures (thus different sites) simultaneously. More particularly, the inhibitory complexes of most effectiveness regarding each ligand opt for more in-depth discussion, which is signified in bold.

Table 3 summarises in-detail data for the selected ligand-3W37 duos; Figure 4 gives the visualization of in-site arrangements and interaction maps. These inhibitory configurations are considered the primary contributors to the inhibitability or in other words the main products of ligand-protein inhibition. Overall, the effectiveness is likely based more on the hydrophobic interactions (viz. van der Waals forces) than on the hydrophilic counterparts (viz. hydrogen-like bonds). From the static-intermolecular standpoint, the most effective inhibitory systems are in the order: D-3W37 (DS -13.0 kcal.mol^{-1}; RMSD 1.17 Å) > 1-3W37 (DS -12.8 kcal.mol^{-1}; RMSD 1.23 Å) > 2-3W37 (DS -12.3 kcal.mol^{-1}; RMSD 1.76 Å) > 11-3W37 (DS -12.0 kcal.mol^{-1}; RMSD 1.20 Å) ≈ 13-3W37 (DS -12.1 kcal.mol^{-1}; RMSD 1.58 Å); in which, DS values are considered as the corresponding pseudo-Gibbs free energy and RMSD values represent complementarity of ligand structure and in-site features.

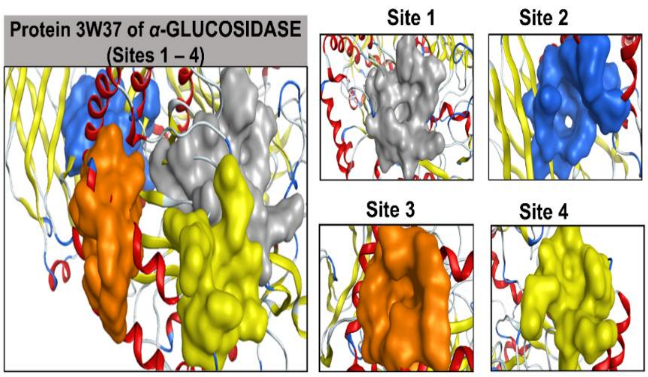

Figure 3: Quaternary structures of protein 3W37 with their approachable sites by the investigated compounds: site 1 (gray), site 2 (blue), site 3 (orange), site 4 (yellow)

ISSN 2616-0684 (Print)
ISSN 2616-0692 (Electronic)

Table 2: Prescreening results on inhibitability of ligands (1–15) and controlled drug Acarbose (D) towards the sites of protein 3W37

C	Site 1		Site 2		Site 3		Site 4		Overall
	E	N	E	N	E	N	E	N	E
1-3W37	-12.8	3	-9.8	1	-9.0	1	-10.7	2	-10.6
2-3W37	-8.9	1	-10.0	2	-9.3	1	-12.3	3	-10.1
3-3W37	-10.0	2	-8.7	1	-7.1	0	-8.0	1	-8.5
4-3W37	-9.8	2	-6.7	0	-7.1	0	-6.5	1	-7.5
5-3W37	-6.2	0	-6.9	0	-7.0	0	-9.1	1	-7.3
6-3W37	-8.1	1	-6.0	0	-7.1	0	-9.7	2	-7.7
7-3W37	-10.2	2	-8.0	1	-7.7	0	-6.9	0	-8.2
8-3W37	-10.1	2	-6.0	0	-6.2	0	-7.1	1	-7.4
9-3W37	-11.0	3	-10.3	2	-8.3	1	-8.7	1	-9.6
10-3W37	-11.3	3	-9.0	1	-9.5	1	-9.1	1	-9.7
11-3W37	-12.0	3	-8.8	1	-9.1	1	-10.4	2	-10.1
12-3W37	-9.3	1	-8.0	1	9.2	1	-11.7	3	-5.0
13-3W37	-10.9	2	-10.7	2	-8.6	1	-12.1	3	-10.6
14-3W37	-9.2	1	-8.5	1	-9.6	1	-11.4	3	-9.7
15-3W37	-10.3	2	-8.0	1	-9.9	2	-11.0	3	-9.8
D-3W37	-11.0	2	-13.0	5	-10.8	2	-11.9	3	-11.7

C: Complex; E: DS value (kcal.mol^{-1}); N: Number of hydrophilic interactions

Table 3: Detailed molecular docking simulation results for ligand-3W37 inhibitory complexes

Ligand-protein complex			Hydrogen bond						van der Waals interaction
Name	DS	RMSD	L	P		T	D	E	
1-3W37	-12.8	1.23	O	S	MET 470	H-donor	3.36	-0.7	Lys 506, Asp 232, Ile 233, Phe 476, Arg 552, Asp 568, Gly 567, Trp 565, His 626, Ile 396, Asp 357, Phe 601, Trp 467, Asp 469, Phe 236, Trp 432
			O	N	ALA 234	H-acceptor	2.99	-1.9	
			C	6-ring	TRP 329	H-π	4.74	-0.7	
2-3W37	-12.3	1.76	C	O	ASP 568	H-donor	3.26	-1.2	Asp 232, Ser 474, Arg 552, Asp 469, Trp 467, Trp 565, Phe 601, Asp 357, Ile 396, Met 470, Trp 432
			O	N	LYS 506	H-acceptor	3.32	-1.0	
			C	6-ring	PHE 476	H-π	3.59	-0.7	
3-3W37	-10.0	0.77	O	S	MET 470	H-donor	3.82	-0.4	Ala 234, Arg 552, Phe 236, Trp 329, Phe 601, Asp 357, Ile 396, Trp 467, His 626, Asp 469, Asp 568, Asp 232, Trp 432
			O	N	LYS 506	H-acceptor	2.97	-1.7	
4-3W37	-9.8	1.07	C	S	MET 470	H-donor	4.03	-0.8	Lys 506, Ser 430, Phe 476, Arg 552, Trp565, Asp 568, Asp 232, Trp 432, Gly 567, Asp 469, Asp 357, Phe 601, Trp 329
			O	S	MET 470	H-donor	3.42	-0.9	
5-3W37	-9.1	0.94	O	O	MET 361	H-donor	2.91	-2.3	Tyr 331, His 633, Arg 629, Gly 330, Arg 328, Glu 336, Arg 332, Asp 359, Ala 363, Asp 362, Phe 364, Aps 370, His 373, Phe 374
6-3W37	-9.7	1.92	O	O	ASP 370	H-donor	2.78	-3.1	Gly 330, Tyr 331, Asp 359, Arg 629, Arg 332, Phe 364, Asp 362, His 373
			O	N	ALA 363	H-acceptor	3.10	-0.3	
7-3W37	-10.2	1.87	O	O	ASP 232	H-donor	2.93	-1.4	Lys 506, Ile 233, Arg 552, Asp 568, Ile 396, Asp 357, Trp 432, Phe 601, Trp 329, Asp 269, Met 470, Ile 358
			C	6-ring	PHE 476	H-π	3.96	-1.0	

ISSN 2616-0684 (Print)
ISSN 2616-0692 (Electronic)

8-3W37	-10.1	1.33	O	O	ASP 357	H-donor	3.12	-0.8	Asp 630, Glu 603, Phe 236, Ala 602, Ala 234, Ala 628, Trp 329, Asp 568, Phe 601, Ile 396, Asp 469, Trp 432, Arg 552, Asp 232
			O	S	MET 470	H-donor	3.22	-2.0	
9-3W37	-11.0	1.26	O	S	MET 470	H-donor	3.62	-1.0	Phe 236, Ala 628, Phe 601, Trp 329, Ile 396, Asp 357, Arg 552, Asp 568, Ala 234, Asp 232, Asp 469, Phe 476
			O	N	TRP 432	H-acceptor	2.87	-1.1	
			O	N	LYS 506	H-acceptor	2.83	-5.6	
10-3W37	-11.3	1.52	O	O	ASP 568	H-donor	2.76	-2.6	Asp 232, Arg 552, Trp 432, Trp 565, Trp 467, Ile 396, Phe 601, Asp 469, Met 470, Lys 506, Phe 476, Trp 329
			O	O	ASP 357	H-donor	2.97	-1.8	
			O	O	ASP 357	H-donor	3.27	-0.8	
11-3W37	-12.0	1.20	O	N	LYS 506	H-acceptor	3.11	-1.1	Arg 552, Phe 236, Trp 329, Phe 601, Asp 568, Ile 358, Asp 357, Ile 396, Trp 432, Met 470
			C	6-ring	PHE 476	H-π	4.24	-0.6	
			C	6-ring	PHE 476	H-π	4.01	-0.7	
12-3W37	-11.7	0.95	O	N	ARG 629	H-acceptor	3.05	-0.7	Asp 370, Phe 374, Val 372, Arg 332, Gly 330, Tyr 331, Asp 359, Met 361, Ala 363
			C	5-ring	HIS 373	H-π	3.90	-0.8	
			C	6-ring	PHE 364	H-π	4.22	-0.9	
13-3W37	-12.1	1.58	O	C	ARG 332	H-acceptor	3.43	-0.6	Gly 330, Asp 359, Ala 363, Phe 364, Phe 374, Met 361, His 373, Asp 370, Tyr 331
			O	N	ARG 629	H-acceptor	3.18	-1.3	
			O	N	ARG 629	H-acceptor	3.14	-1.2	
14-3W37	-11.4	1.12	O	O	ASP 359	H-donor	3.07	-0.7	Ala 363, Met 361, His 373, Tyr 331, Phe 364, Asp 370
			O	N	ARG 629	H-acceptor	3.20	-2.0	
			O	C	ARG 332	H-acceptor	3.49	-0.7	
15-3W37	-11.0	1.64	O	C	ARG 332	H-acceptor	3.38	-0.8	Ala 363, Arg 629, Phe 364, Asp 359, Tyr 331, Met 361, Gly 330, Asp 370
			C	5-ring	HIS 373	H-π	4.47	-0.8	
			O	5-ring	HIS 373	H-π	3.81	-2.0	
D-3W37	-13.0	1.17	O	O	Glu 792	H-donor	3.20	-0.7	Asp 666, Arg 670, Thr 299, Pro 683, Glu 301, Phe 680, Arg 814, Thr 681, Gly 698, Leu 663, Gly 700, Asn 758, Thr 790, Tyr 659, Val 760, Gly 791
			O	O	Ile 759	H-donor	2.77	-2.1	
			O	N	Arg 699	H-acceptor	2.77	-4.4	
			O	N	Arg 699	H-acceptor	3.23	-1.7	
			O	N	Arg 676	H-acceptor	2.99	-0.6	

DS: Docking score energy ($kcal.mol^{-1}$); RMSD: Root-mean-square deviation (Å); L: Ligand; P: Protein; T: Type; D: Distance (Å); E: Energy ($kcal.mol^{-1}$)

It noteworthy that these retrievals are based on static interaction algorithm, thus omitting the kinetics of the atoms when in interactions with each other. As suggestions, the missing information can be acquired using molecular dynamics technique or validated with surface plasmon resonance characterisation. In 2D maps, dashed arrows are hydrogen-like bonds, blurry purple shows van de Waals interactions, and dashed contours indicates conformational fitness. In 3D renderings, the sites appear to be open and large compared to the inhibitors; as the results, this implies that further modification on the current structures are highly practicable. In other words, the size increase might not significantly deter their ability to be folded into the inhibitory sites. If subjected to a nonequivalent reference to our experiment-correlated works on single-enzymatic inhibition, these values might be referred to as effective inhibitors against α-glucosidase (assaying-based IC_{50} values < 100 μM).[37,38] Therefore, the *G. lucidum* extracts, in general, and 1 (Butyl lucidenate P), 2 (Butyl lucidenate E_2), 11 (Methyl ganoderate H), 13 (Methyl lucidenate N), in particular, are highly recommended for further experimental validation from enzymatic bioassays.

QSARIS-based physicochemical properties

The parameters are retrieved to Table 4, including those from the QSARIS system and the number of hydrogen bonds (counted from docking-based results). Overall, all the inhibition-effective candidates (1, 2, 11, 13) predicted by molecular docking simulation are also suitable for biocompatible applications. The compounds reasonably suffice Lipinski's criteria, i.e.: (i) molecular mass ~ 500 amu; (ii) log*P* 2-4; (iii) total hydrogen-like counts < 3 (either donating or accepting). Furthermore, the structures possess significant polarisability, which by definition represents the sensitivity to external electric fields; for example, those are created by other polarised agents, e.g. amino-acid-based protein structures. This property, to a certain extent, evaluates the ability of the compounds to break through the solvation double layers, particularly ranked into the order 11 (59.3 $Å^3$) > 1 (56.7 $Å^3$) > 2 (52.1 $Å^3$) > 13 (50.8 $Å^3$). The unit conversion is given by Claussius-Mossotti relation: $10^6/4\pi\epsilon_0\ [A^2.s^4.kg^{-1}] \equiv 1\ [cm^3]$.[39] Also, their low octanol/water partition coefficients, especially 11 (log*P* 2.07) and 13 (log*P* 2.76), are conducive to their aqueous transportability, such as biological media. Therefore, the potentiality of 1 (Butyl lucidenate P), 2 (Butyl lucidenate E_2), 11 (Methyl ganoderate H), and 13 (Methyl lucidenate N) is highly justified from the standpoint of biocompatibility and drug-likeness (by Lipinski's rule of five).

ADMET-based pharmacokinetics and pharmacology

The pharmacokinetic and pharmacological indicators (absorption, distribution, metabolism, excretion, and toxicity) of the *G. lucidum* extract components are given in Table 5 (1-8) and Table 6 (9-15, D). Overall, all the compounds are considered safe and effective for use in pharmaceutical applications, thus the total extract is in general; the specific arguments are discussed as following. Given intestinal absorption, they are expected to be absorbed almost completely with > 80 % (Acarbose ca. 4 %; recommended > 30 %); their log Papp values > 0.7 are translated to high Caco-2 permeability, which means low intestinal resistance, thus promising as orally administered drugs. Most of the compounds are predicted to be flushed out of the cell by P-glycoprotein, yet also able to inhibit the protein family; this means they can enhance the bioavailability of other intra-cellular drugs by reducing the activity of the membrane-based proteins.

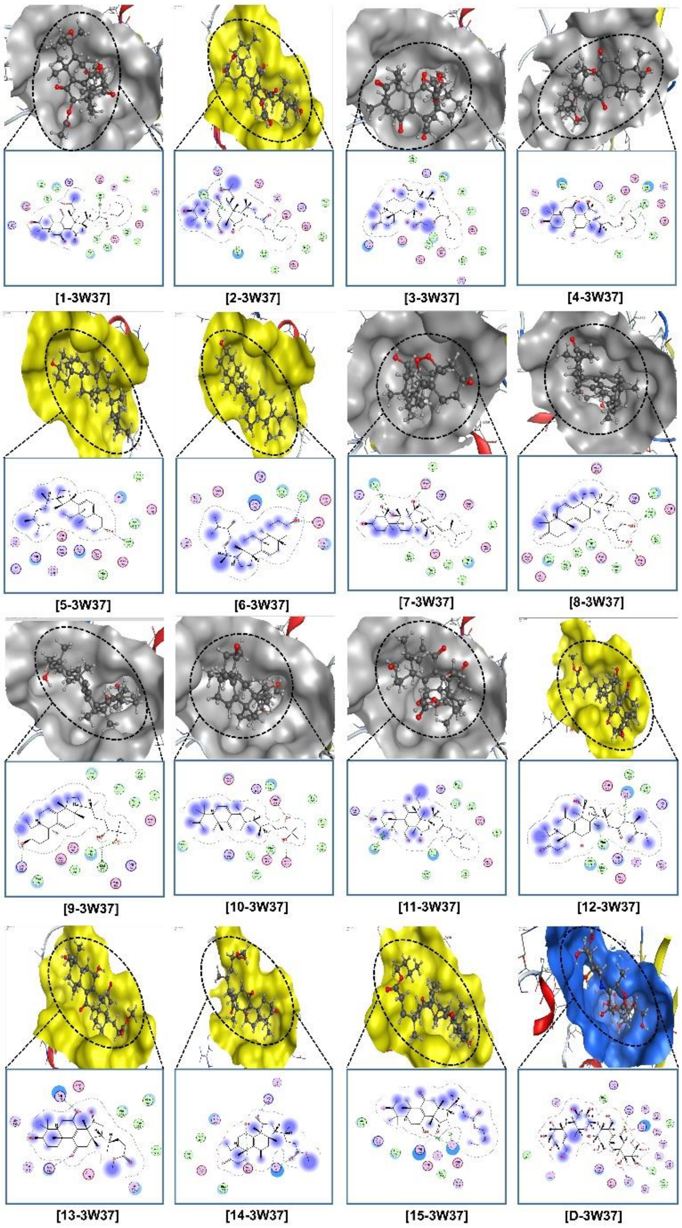

Figure 4: In-pose interaction map of inhibitory complexes between 1–15, D and 3W37

Regarding distribution, the *G. lucidum* composition is balanced and presented in blood plasma and tissues (by VDss), partially crossing the blood-brain barrier (by BBB permeability) and penetrating the central neural system (by CNS permeability). In terms of metabolism, all the candidates are able to be metabolized by the cytochrome P450 (specifically, CYP3A4); however, none of them is predicted to inhibit the enzymatic activities, thus no interrupting the metabolic activities of the body. Also, most compounds (except for 6) are unlikely to be excreted by renal OCT2. Finally, high safety is expected, especially regarding those with the highest inhibitory prediction (viz. 1, 2, 11, 13): no mutagenic risk (AMES toxicity); no restriction on the potassium channels (as hERG I and II inhibitors); no liver-harmful potential (i.e. hepatotoxicity); no skin sensitization; toxigenic induction towards bacteria (e.g. *T. Pyriformis*) yet safety to higher forms of organisms (e.g. Flathead Minnow fish). Therefore, the pharmacokinetics and pharmacology retrieved further justify the selection of 1 (Butyl lucidenate P), 2 (Butyl lucidenate E_2), 11 (Methyl ganoderate H), and 13 (Methyl lucidenate N) for pharmaceutical applications in general and for oral-taken products in particular.

DFT-based chemical properties

The results from quantum calculation are considered as *ab initio* insights of chemical properties of the candidates, thus can be used for the argument on their bio-medium compatibility and intermolecular interactability.

The optimised geometries of the bioactive compounds are shown in Figure 5. Overall, the input structures can be self-consistently converged easily without any geometrical constraints or abnormal bonding parameters (i.e. angles and length). To common view, natural compounds are often known without noticeable constraints in their chemical structure; to another view, the results obtained from geometrical optimisation, to certain degree, can validate spectroscopic characterisation and structural elucidation from the preceding works.

The corresponding molecular properties are summarised in Table 7, including ground state energy and dipole moment. In principle, the former equals the molecular stability, i.e. the chemical activeness in general; while, the latter is the positive-negative charge separation in a system, thus measuring the compatibility with a dipole-solvent environment, such as physio-chemical media. Overall, all ground-state energies register negative values (under -1000 a.u.). This means that the molecules are less likely to be sensitive to chemical reacting attacks; in other words, the compounds are more likely to retain their structural elements in biological media before reaching the targeted protein and serving as bio-inhibitors. In terms of dipole moment, the figures vary significantly from 2 to 10 Debye, indicating a broad range of dipole-environment compatibility. More particularly, the promising candidates also possess predominant figures of ground-state energy, ranked in the order: 11 (-1961.62 a.u.) > 1 ≈ 2 (ca. -1900 a.u.) > 13 (-1543.14 a.u); also, they register the dipole moment values of significance, i.e.: 1 (9.129 Debye) > 13 (8.294 Debye) > 2 (6.689 Debye) > 11 (5.106 Debye). In contrast, the energy value of 5 (-1089.74 a.u.) can be translated into highest susceptibility to chemical reaction; while, the dipole moment of 6 (2.054 Debye) can be interpreted as lowest biological compatibility. Furthermore, although 4 (with its dipole moment of 10.292 Debye) might hold pronounced bio-suitable potentiality, docking-based simulation already indicated that it is unlikely to be an effective inhibitor against α-glucosidase.

The highest occupied molecular orbital (HOMO) and lowest unoccupied molecular orbital (LUMO) of the studied structures are shown in Figure 6, with their band-gap energy (ΔE_{GAP}). The value can be considered as an indicator for the intermolecular binding capability towards protein structures since the polypeptide molecules was known and proved with electric conductivity, explained by electron tunneling mechanism.[40] Simply put, the lower is the better. Overall, the values vary widely between 3.5 and 6.5 eV, lying within the transition range between an insulator (> 9 eV) and a semiconductor (< 3.2 eV). In particular, the promising candidates can be argued for their protein-bound potential into the order: 11 (3.599 eV) > 13 (4.598 eV) > 1 (5.952 eV) > 2 (6.393 eV). Amongst all compounds, only 12 (3.523 eV) is comparable to the first one yet especially discouraged by docking-based algorithms.

Table 4: Physicochemical properties of studied compounds 1–15 and the controlled drug D

Compound	Mass (amu)	Polarisability (Å^3)	Size (Å)	Dispersion coefficients		Hydrogen bond (3W37)		
				log*P*	log*S*	H-donor	H-acceptor	H-*π*
1	573.8	56.7	823.4	3.89	-4.01	1	1	1
2	572.0	52.1	814.4	3.03	-4.08	1	1	1
3	571.2	57.6	821.8	3.17	-4.76	1	1	0
4	515.1	53.8	756.5	3.20	-4.63	2	0	0
5	398.1	44.2	654.3	5.08	-6.89	1	0	0
6	397.5	46.4	664.3	6.04	-7.09	1	1	0
7	426.8	50.9	623.0	5.67	-6.07	1	0	1
8	454.3	52.7	690.6	4.03	-5.01	2	0	0
9	458.2	50.2	689.9	5.09	-5.06	1	2	0
10	457.1	51.7	710.5	4.43	-5.63	3	0	0
11	586.0	59.3	768.1	2.07	-3.82	0	1	2
12	528.2	55.8	735.4	1.39	-3.10	0	1	2
13	472.9	50.8	669.1	2.76	-3.67	0	3	0
14	473.1	50.2	624.2	2.13	-3.35	1	2	0
15	514.7	55.3	752.3	4.07	-4.49	0	1	2
D	645.9	60.7	614.1	2.74	-0.93	2	3	0

Table 5: ADMET-based pharmacokinetic and pharmacology of the studied compounds 1–8

Property	1	2	3	4	5	6	7	8	Unit
Absorption									
Water solubility	-4.725	-4.761	-4.677	-4.613	-7.092	-7.121	-5.763	-6.392	(1)
Caco2 permeability	0.774	0.824	0.848	0.803	1.297	1.296	1.156	1.249	(2)
Intestinal absorption	82.127	87.411	92.695	88.91	96.402	96.255	92.678	95.212	(3)
Skin Permeability	-2.961	-3.003	-2.833	-2.849	-2.759	-2.758	-3.904	-3.3	(4)
P-glycoprotein substrate	Yes	Yes	No	Yes	No	No	Yes	Yes	(5)
P-glycoprotein I inhibitor	Yes	Yes	Yes	Yes	Yes	Yes	Yes	Yes	(5)
P-glycoprotein II inhibitor	Yes	Yes	Yes	Yes	Yes	Yes	Yes	Yes	(5)
Distribution									
VDss	0.095	0.176	0.075	0.014	0.326	0.328	0.334	-0.108	(6)
Fraction unbound	0.063	0.026	0.012	0.011	0	0	0	0	(6)
BBB permeability	-0.811	-0.973	-1.051	-0.441	0.797	0.794	-0.199	-0.242	(7)
CNS permeability	-2.871	-2.821	-2.78	-2.817	-1.376	-1.376	-1.841	-1.693	(8)
Metabolism									
CYP2D6 substrate	No	No	No	No	No	No	No	No	(5)
CYP3A4 substrate	Yes	Yes	Yes	Yes	Yes	Yes	Yes	Yes	(5)
CYP1A2 inhibitior	No	No	No	No	No	No	No	No	(5)
CYP2C19 inhibitior	No	No	No	No	No	No	No	No	(5)
CYP2C9 inhibitior	No	No	No	No	No	No	No	No	(5)
CYP2D6 inhibitior	No	No	No	No	No	No	No	No	(5)
CYP3A4 inhibitior	Yes	Yes	No	No	No	No	No	No	(5)
Excretion									
Total Clearance	0.405	0.333	0.281	0.43	0.564	0.563	0.598	0.504	(9)
Renal OCT2 substrate	No	No	No	No	No	No	Yes	No	(5)

 ISSN 2616-0684 (Print)
ISSN 2616-0692 (Electronic)

Toxicity									
AMES toxicity	No	No	No	No	No	No	No	No	(5)
Max. tolerated dose	-0.374	-0.12	0.168	-0.342	-0.242	-0.237	-0.552	-1.047	(10)
hERG I inhibitor	No	No	No	No	No	No	No	No	(5)
hERG II inhibitor	No	No	No	No	Yes	Yes	No	No	(5)
Oral Rat Acute Toxicity (LD50)	2.551	2.372	1.874	3.022	2.323	2.329	2.136	3.824	(11)
Oral Rat Chronic Toxicity (LOAEL)	2.04	0.851	0.924	1.585	1.142	1.142	1.563	2.001	(12)
Hepatotoxicity	No	No	No	No	No	No	Yes	Yes	(5)
Skin Sensitisation	No	No	No	No	No	No	No	No	(5)
T.Pyriformis toxicity	0.286	0.287	0.287	0.301	0.683	0.68	0.363	0.591	(13)
Minnow toxicity	1.272	1.004	0.818	0.61	-1.901	-1.944	0.018	0.845	(14)

(1) log $mol.L^{-1}$; (2) log Papp (10^{-6} $cm.s^{-1}$); (3) %; (4) log Kp; (5) Yes/No; (6) log $L.kg^{-1}$; (7) log BB; (8) log PS;
(9) log $mL.min^{-1}.kg^{-1}$; (10) log $mg.kg^{-1}.day^{-1}$; (11) $mol.kg^{-1}$; (12) log $mg.kg^{-1}$_bw.day^{-1}; (13) log $\mu g.L^{-1}$; (14) log mM

Table 6: ADMET-based pharmacokinetic and pharmacology of the studied compounds 9−15 and D

Property	**9**	**10**	**11**	**12**	**13**	**14**	**15**	**D**	**Unit**
Absorption									
Water solubility	-5.814	-6.291	-4.422	-4.346	-4.342	-4.236	-4.693	-1.482	(1)
Caco2 permeability	1.161	1.172	0.838	0.875	0.799	0.832	0.779	-0.481	(2)
Intestinal absorption	91.438	93.963	86.715	93.498	86.574	91.859	88.91	4.172	(3)
Skin Permeability	-3.045	-3.243	-2.928	-3.063	-3.603	-3.404	-3.168	-2.735	(4)
P-glycoprotein substrate	Yes	Yes	Yes	No	Yes	Yes	Yes	Yes	(5)
P-glycoprotein I inhibitor	Yes	Yes	Yes	Yes	Yes	Yes	Yes	No	(5)
P-glycoprotein II inhibitor	Yes	Yes	Yes	Yes	Yes	Yes	Yes	No	(5)
Distribution									
VDss	-0.024	0	0.207	0.069	-0.056	-0.106	-0.039	-0.836	(6)
Fraction unbound	0	0	0.093	0.06	0.132	0.126	0.054	0.505	(6)
BBB permeability	-0.155	-0.117	-1.154	-0.676	-0.357	-0.421	-0.429	-1.717	(7)
CNS permeability	-1.6	-1.525	-2.848	-2.798	-2.851	-2.81	-2.839	-6.438	(8)
Metabolism									
CYP2D6 substrate	No	No	No	No	No	No	No	No	(5)
CYP3A4 substrate	Yes	Yes	Yes	Yes	Yes	Yes	Yes	No	(5)
CYP1A2 inhibitior	No	No	No	No	No	No	No	No	(5)
CYP2C19 inhibitior	No	No	No	No	No	No	No	No	(5)
CYP2C9 inhibitior	No	No	No	No	No	No	No	No	(5)
CYP2D6 inhibitior	No	No	No	No	No	No	No	No	(5)
CYP3A4 inhibitior	No	No	Yes	Yes	Yes	No	No	No	(5)
Excretion									
Total Clearance	0.388	0.335	0.209	0.229	0.409	0.362	0.424	0.428	(9)
Renal OCT2 substrate	No	No	No	No	No	No	No	No	(5)
Toxicity									
AMES toxicity	No	No	No	No	No	No	No	No	(5)
Max. tolerated dose (human)	-0.829	-0.714	0.009	-0.063	-0.386	-0.105	-0.33	0.435	(10)
hERG I inhibitor	No	No	No	No	No	No	No	No	(5)
hERG II inhibitor	No	No	No	No	No	No	No	Yes	(5)
Oral Rat Acute Toxicity (LD50)	3.803	3.561	2.62	3.145	2.625	2.235	2.55	2.449	(11)

ISSN 2616-0684 (Print)
ISSN 2616-0692 (Electronic)

Oral Rat Chronic Toxicity (LOAEL)	1.928	1.905	2.578	1.052	1.674	0.914	1.669	5.319	(12)
Hepatotoxicity	Yes	Yes	No	No	No	No	No	No	(5)
Skin Sensitisation	No	No	No	No	No	No	No	No	(5)
T.Pyriformis toxicity	0.523	0.589	0.285	0.29	0.304	0.307	0.302	0.285	(13)
Minnow toxicity	0.916	0.772	1.935	1.04	0.927	0.741	0.306	16.823	(14)

(1) log mol.L^{-1}; (2) log Papp (10^{-6} cm.s^{-1}); (3) %; (4) log Kp; (5) Yes/No; (6) log L.kg^{-1}; (7) log BB; (8) log PS;

(9) log mL.min^{-1}.kg^{-1}; (10) log mg.kg^{-1}.day^{-1}; (11) mol.kg^{-1}; (12) log mg.kg^{-1}_bw.day^{-1}; (13) log μg.L^{-1}; (14) log mM

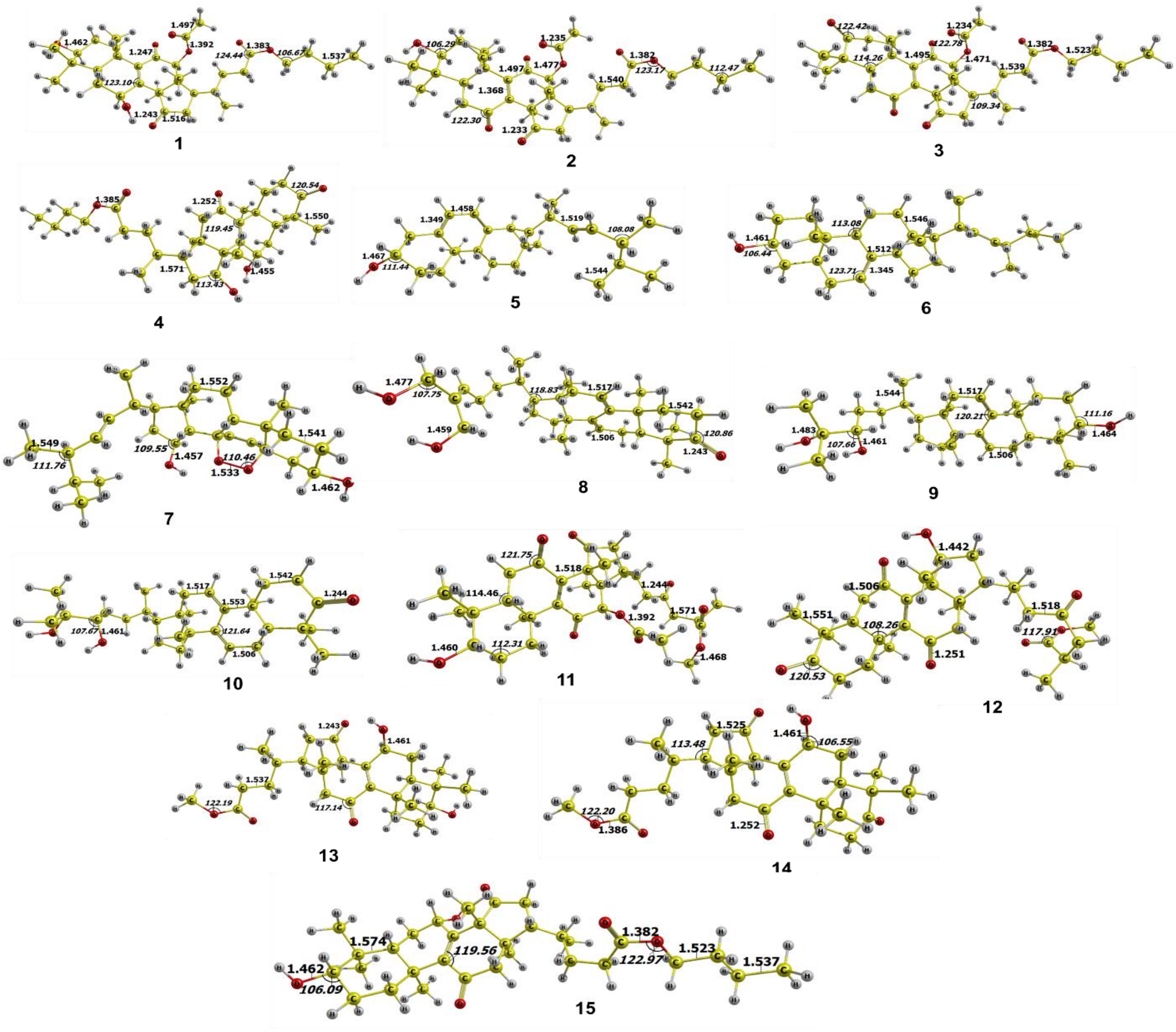

Figure 5: Geometrically optimized structures of 1-15 by DFT at the level of theory M052X/6-311++g(d,p)

Molecular electronic potential (MEP) maps of the structures are given in Figure 7. The conventional shading provides information on the molecular distribution of chemical activities, i.e.: (i) reddish regions are equivalent to the negative electrostatic potential; (ii) bluish regions are equivalent the positive electrostatic potential; (iii) whitish colours are equivalent to the neutral tendency. The compounds can be categorised into two explicit tendencies; particularly, 1-4, 11-15 change their chemical tendencies rather arbitrarily and consecutively over the molecular planes, while those of others are likely to be localised to certain regions or functional groups of the host molecule. This can be seen by the change of regional colours over their molecules. From theoretical standpoint, the former implicates the flexibility when in physical interactions with external complex structures. In other words, the structural features might help the host molecule more adaptable to the surface features of its potential targeted proteins. It is noteworthy that this discussion is more likely interpretative assessment than a quantitative evaluation backed by solid values.

Conclusion

This study specifies the diabetic potentiality of the methanol-extracted components (1-15) of *G. lucidum*. Molecular docking simulation reveals the most effective inhibitory systems to the order: D-3W37 (DS -13.0 kcal.mol^{-1}; RMSD 1.17 Å) > 1-3W37 (DS -12.8 kcal.mol^{-1}; RMSD 1.23 Å) > 2-3W37 (DS -12.3 kcal.mol^{-1}; RMSD 1.76 Å) > 11-3W37 (DS -12.0 kcal.mol^{-1}; RMSD 1.20 Å) > 13-3W37 (DS -12.1 kcal.mol^{-1}; RMSD 1.58 Å). The potentiality of 1 (Butyl lucidenate P), 2 (Butyl lucidenate E$_2$), 11 (Methyl ganoderate H), and 13 (Methyl lucidenate N) is highly justified for drug-like development (by QSARIS-based physicochemical properties in reference to Lipinski's

 ISSN 2616-0684 (Print)
ISSN 2616-0692 (Electronic)

rule of five) and pharmaceutical applications (by ADMET-based pharmacokinetics and pharmacology). Quantum-based calculations provide an additional view from intrinsic chemical properties, including (i) ground-state energy: 11 (-1961.62 a.u.) > 1 ≈ 2 (ca. -1900 a.u.) > 13 (-1543.14 a.u); (ii) dipole moment: 1 (9.129 Debye) > 13 (8.294 Debye) > 2 (6.689 Debye) > 11 (5.106 Debye); (iii) band gap: 11 (3.599 eV) > 13 (4.598 eV) > 1 (5.952 eV) > 2 (6.393 eV). The results altogether contribute to the understanding of *G. lucidum* effects from the theoretical views and encourage further experimental attempts to mass-isolate the promising components for anti-diabetic tests in particular.

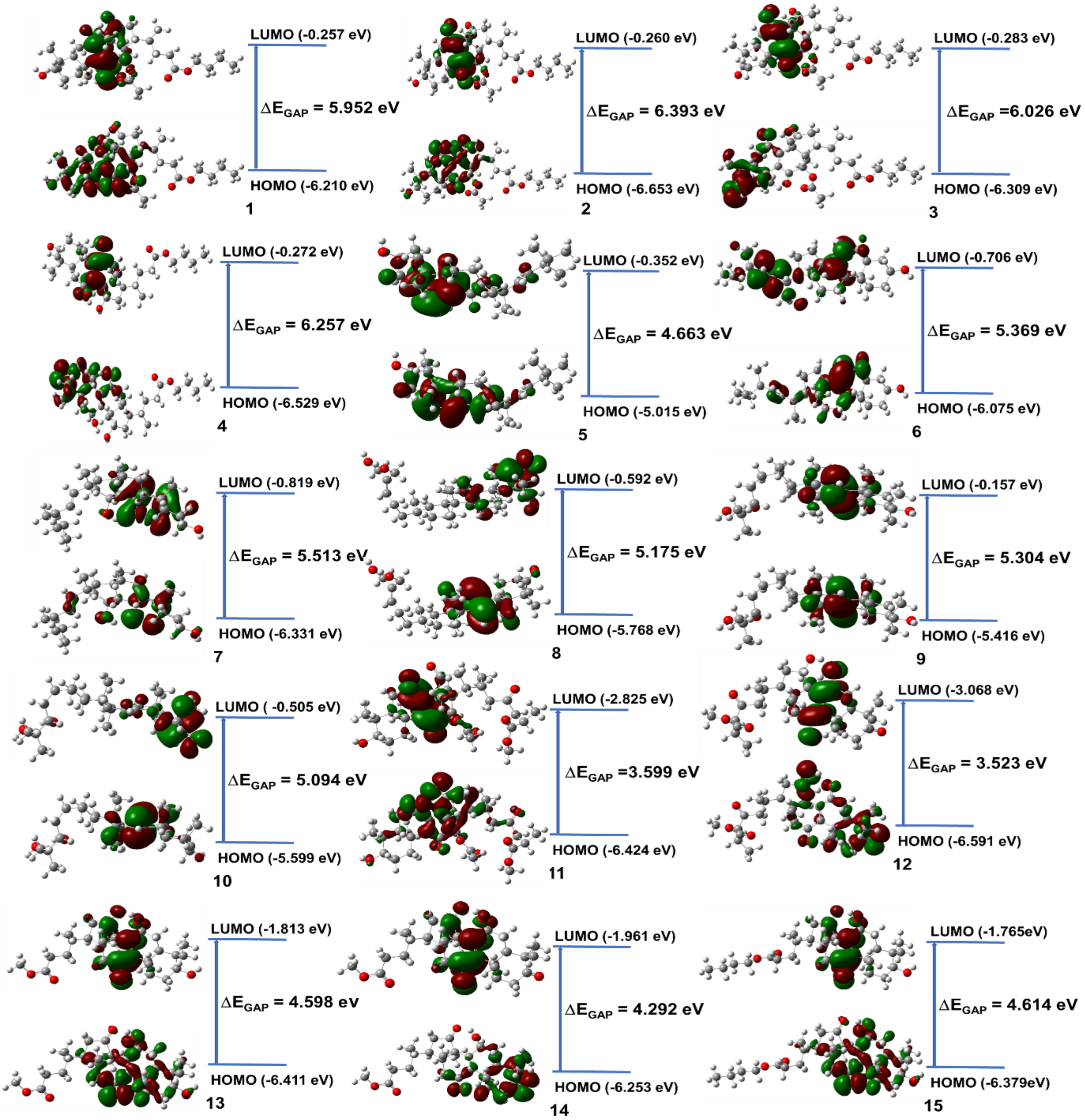

Figure 6: Frontier molecular orbitals (HOMO and LUMO) of 1-15 at the level of theory M052X/def2-TZVPP

Table 7: Ground state electronic energy and dipole moment value of 1–15 by DFT at the level of theory M052X/6-311++g(d,p)

Compound	Ground state electronic energy (a.u.)	Dipole moment (Debye)
1	-1888.85270	9.129
2	-1887.64245	6.689
3	-1886.44224	8.362
4	-1661.06448	10.292
5	-1089.73781	2.263

6	-1169.60142	2.054
7	-1393.86501	3.858
8	-1396.13408	5.699
9	-1398.57930	4.731
10	-1397.37809	5.033
11	-1961.62318	5.106
12	-1733.83558	5.348
13	-1543.14013	8.294
14	-1541.94010	9.487
15	-1661.06095	6.300

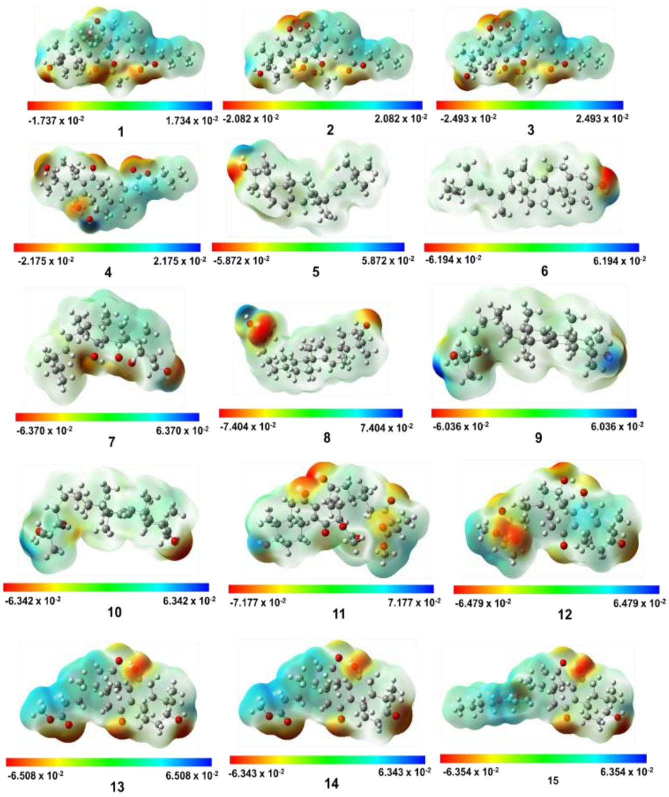

Figure 7. Molecular electrostatic potential (MEP) formed by mapping of total density over the electrostatic potential of 1-15 at the level of theory M052X/def2-TZVPP

Conflict of Interest

The authors declare no conflict of interest.

Authors' Declaration

The authors hereby declare that the work presented in this article is original and that any liability for claims relating to the content of this article will be borne by them.

Acknowledgments

This research was funded for computational research by Hue Unversity [Grant No. DHH2022-01-198]. Nguyen Thi Ai Nhung acknowledges the partial support of Hue University under the Core Research Program [Project No. NCM.DHH.2020.04].

References

1. Pk MMU, Islam MS, Rumana P, Subhajit D, Talukder RI, Soma NJ, Matiar R. Enzyme inhibitory and antioxidant activity of combination of two edible mushrooms of Ganoderma lucidum and Pleurotus ostreatus. Trop J Nat Prod Res. 2018;2(7):314–319.
2. Lee MK, Hung TM, Cuong TD, Na M, Kim JC, Kim E, Park H, Choi JS, Lee I, Bae K. Ergosta-7, 22-diene-2β, 3α, 9α-triol from the Fruit Bodies of Ganoderma lucidum Induces Apoptosis in Human Myelocytic HL-60 Cells. Phyther Res. 2011;25(11):1579–1585.
3. Tung NT, Cuong TD, Hung TM, Kim JA, Woo MH, Choi JS, Lee JH, Min BS. Cytotoxic and anti-angiogenic effects of lanostane triterpenoids from Ganoderma lucidum. Phytochem Lett. 2015;12:69–74.
4. Tung NT, Cuong TD, Hung TM, Lee JH, Woo MH, Choi JS, Kim J, Ryu SH, Min BS. Inhibitory effect on NO production of triterpenes from the fruiting bodies of Ganoderma lucidum. Bioorg Med Chem Lett. 2013;23(5):1428–1432.
5. Chen B, Tian J, Zhang J, Wang K, Liu L, Yang B, Bao L, Liu H. Triterpenes and meroterpenes from Ganoderma lucidum with inhibitory activity against HMGs reductase, aldose reductase and α-glucosidase. Fitoterapia. 2017;120:6–16.
6. Yang C, Li W, Li C, Zhou Z, Xiao Y, Yan X. Metabolism of ganoderic acids by a Ganoderma lucidum cytochrome P450 and the 3-keto sterol reductase ERG27 from yeast. Phytochemistry. 2018;155:83–92.
7. Zhao XR, Huo XK, Dong PP, Wang C, Huang SS, Zhang BJ, Zhang HL, Deng S, Liu KX, Ma XC. Inhibitory effects of highly oxygenated lanostane derivatives from the fungus Ganoderma lucidum on P-glycoprotein and α-glucosidase. J Nat Prod. 2015;78(8):1868–1876.
8. Fan J, Fu A, Zhang L. Progress in molecular docking. Quant Biol. 2019;7(2):83–89.
9. Quy PT, Bui TQ, Bon N V, Phung PTK, Duc DPN, Nhan DT, Phu N V, To DC, Nhung NTA. Euonymus laxiflorus Champ. Bioactive Compounds Inhibited α-Glucosidase and Protein Phosphatase 1B – A Computational Approach Towards the Discovery of Antidiabetic Drugs. Trop J Nat Prod Res Available. 2023;7(5):2974–2991.
10. Chatterjee S, Khunti K, Davies MJ. Type 2 diabetes. Lancet. 2017;389(10085):2239–2251.
11. Rabasa-Lhoret R, Chiasson J. α-Glucosidase inhibitors. Int Textb diabetes Mellit. 2003;
12. Kimura A, Lee JH, Lee IS, Lee HS, Park KH, Chiba S, Kim D. Two potent competitive inhibitors discriminating α-glucosidase family I from family II. Carbohydr Res. 2004;339(6):1035–1040.
13. Goad LJ, Akihisa T. Mass spectrometry of sterols. In: Analysis of Sterols. Springer; 1997. page 152–196.
14. Cambie RC, Le Quesne PW. Chemistry of fungi. Part III. Constituents of Coriolus sanguineus Fr. J Chem Soc C Org. 1966;72–4.

ISSN 2616-0684 (Print)
ISSN 2616-0692 (Electronic)

15. Kikuchi T, Kanomi S, Murai Y, Kadota S, Tsubono K, Ogita ZI. Constituents of the Fungus Ganoderma lucidum (FR.) KARST. II.: Structures of Ganoderic acids F, G, and H, Lucidenic acids D2 and E2, and related compounds. Chem Pharm Bull. 1986;34(10):4018–4029.
16. Nishitoba T, Oda K, Sato H, Sakamura S. Novel triterpenoids from the fungus Ganoderma lucidum. Agric Biol Chem. 1988;52(2):367–372.
17. Fujita A, Arisawa M, Saga M, Hayashi T, Morita N. Two new lanostanoids from Ganoderma lucidum. J Nat Prod. 1986;49(6):1122–1125.
18. Xiangli Z, Haiying B. Advances of Researches on Triterpene Constituents and Pharmacology of Ganoderma lucidum. J Fungal Res. 2004;2(1):68–77.
19. Lee I, Kim H, Youn U, Kim J, Min B, Jung H, Na M, Hattori M, Bae K. Effect of lanostane triterpenes from the fruiting bodies of Ganoderma lucidum on adipocyte differentiation in 3T3-L1 cells. Planta Med. 2010;76(14):1558–1563.
20. Kikuchi T, Kanomi S, Kadota S, Murai Y, Tsubono K, Ogita ZI. Constitutents of the fungus Ganoderma lucidum (FR.) KARST. I.: structures of ganoderic acids C2, E, I, and K, lucidenic acid F and related compounds. Chem Pharm Bull. 1986;34(9):3695–3712.
21. World Health Organization. Global report on diabetes. Geneva, Switzeland: WHO Press; 2016.
22. Sabuhom P, Subin P, Luecha P, Nualkaew S, Nualkaew N. Effects of Plant Part Substitution in a Thai Traditional Recipe on α-Glucosidase Inhibition. Trop J Nat Prod Res. 2023;7(5):2919–2925.
23. Barber E, Houghton MJ, Williamson G. Flavonoids as human intestinal α-glucosidase inhibitors. Foods. 2021;10(8):Article ID 1939.
24. DiNicolantonio JJ, Bhutani J, O'Keefe JH. Acarbose: safe and effective for lowering postprandial hyperglycaemia and improving cardiovascular outcomes. Open Hear. 2015;2(1):Article ID e000327.
25. Zhang F, Xu S, Tang L, Pan X, Tong N. Acarbose with comparable glucose-lowering but superior weight-loss efficacy to dipeptidyl peptidase-4 inhibitors: a systematic review and network meta-analysis of randomized controlled trials. Front Endocrinol (Lausanne). 2020;11:Article ID 00288.
26. McIver LA, Tripp J. Acarbose. US National Library of Medicines, National Institutes of Health. 10 Aug 2020.
27. Molecular Operating Environment (MOE), 2015.02 Chemical Computing Group ULC, 1010 Sherbooke St. West, Suite #910, Montreal, QC, Canada, H3A 2R7, 2015.
28. Tarasova O, Poroikov V, Veselovsky A. Molecular Docking Studies of HIV-1 Resistance to Reverse Transcriptase Inhibitors: Mini-Review. Molecules. 2018;23(5):11–13.
29. Thai KM, Le DP, Tran NVK, Nguyen TTH, Tran TD, Le MT. Computational assay of Zanamivir binding affinity with original and mutant influenza neuraminidase 9 using molecular docking. J Theor Biol. 2015;385:31–39.
30. Ngo T Du, Tran TD, Le MT, Thai KM. Computational predictive models for P-glycoprotein inhibition of in-house chalcone derivatives and drug-bank compounds. Mol Divers. 2016;20(4):945–961.
31. Gasteiger J, Marsili M. Iterative partial equalization of orbital electronegativity-a rapid access to atomic charges. Tetrahedron. 1980;36(22):3219–3228.
32. Lipinski CA, Lombardo F, Dominy BW, Feeney PJ. Experimental and computational approaches to estimate solubility and permeability in drug discovery and development settings. Adv Drug Deliv Rev. 1997;23:3–25.
33. Pires DEV, Blundell TL, Ascher DB. pkCSM: Predicting small-molecule pharmacokinetic and toxicity properties using graph-based signatures. J Med Chem. 2015;58(9):4066–4072.
34. Gaussian 09, Revision A.02, M. J. Frisch, G. W. Trucks, H. B. Schlegel, G. E. Scuseria, M. A. Robb, J. R. Cheeseman, G. Scalmani, V. Barone, G. A. Petersson, H. Nakatsuji, X. Li, M. Caricato, A. Marenich, J. Bloino, B. G. Janesko, R. Gomperts, B. Mennucci.
35. Hohenstein EG, Chill ST, Sherrill CD. Assessment of the performance of the M05− 2X and M06− 2X exchange-correlation functionals for noncovalent interactions in biomolecules. J Chem Theory Comput. 2008;4(12):1996–2000.
36. Reed AE, Weinstock RB, Weinhold F. Natural population analysis. J Chem Phys. 1985;83(2):735–746.
37. Thao TTP, Bui TQ, Hai NTT, Huynh LK, Quy PT, Bao NC, Dung NT, Chi NL, Van Loc T, Smirnova IE. Newly synthesised oxime and lactone derivatives from Dipterocarpus alatus dipterocarpol as anti-diabetic inhibitors: experimental bioassay-based evidence and theoretical computation-based prediction. RSC Adv. 2021;11(57):35765–35782.
38. Thao TTP, Bui TQ, Quy PT, Bao NC, Van Loc T, Van Chien T, Chi NL, Van Tuan N, Van Sung T, Nhung NTA. Isolation, semi-synthesis, docking-based prediction, and bioassay-based activity of Dolichandrone spathacea iridoids: new catalpol derivatives as glucosidase inhibitors. RSC Adv. 2021;11(20):11959–11975.
39. Feynman R. The Feynman lectures on physics - Volume II. Millenium. Gottlieb MA, editor. New York: Basic Books; 2010. 11.3.
40. Cordes M, Giese B. Electron transfer in peptides and proteins. Chem Soc Rev. 2009;38(4):892–901.